Control of the Release of Freely Diffusing Molecules in Single-Cell Electroporation

ARTICLE *in* ANALYTICAL CHEMISTRY · OCTOBER 2009

Impact Factor: 5.64 · DOI: 10.1021/ac9010292 · Source: PubMed

5 AUTHORS, INCLUDING:

Owe Orwar
Karolinska Institutet
158 PUBLICATIONS **5,355** CITATIONS
SEE PROFILE

Stephen Gregory Weber
University of Pittsburgh
233 PUBLICATIONS **3,560** CITATIONS
SEE PROFILE

Published in final edited form as:
Anal Chem. 2009 October 1; 81(19): 8001–8008. doi:10.1021/ac9010292.

Control of the Release of Freely Diffusing Molecules in Single-Cell Electroporation

Aparna Agarwal[†], **Manyan Wang**[†], **Jessica Olofsson**[‡], **Owe Orwar**[‡], and **Stephen G. Weber**[*,†]

Department of Chemistry, University of Pittsburgh, Pittsburgh, Pennsylvania 15260, and Department of Physical Chemistry, Chalmers University of Technology, Kemivägen 10, SE-412 96 Gothenburg, Sweden

Abstract

Single-cell electroporation using an electrolyte-filled capillary is an emerging technique for transient pore formation in adherent cells. Because adherent cells do not have a simple and consistent shape and because the electric field emanating from the tip of the capillary is inhomogeneous, the Schwan equation based on spherical cells in homogeneous electrical fields does not apply. We sought to determine experimental and cell parameters that influence the outcome of a single-cell electroporation experiment. A549 cells were exposed to the thiol-reactive dye Thioglo-1, leading to green fluorescence from intracellular thiol adducts. Electroporation causes a decrease with time of the intracellular fluorescence intensity of Thioglo-1-loaded cells from diffusive loss of thiol adducts. The transient curves thus obtained are well-described by a simple model originally developed by Puc et al. We find that the final fluorescence following electroporation is related to the capillary tip-to-cell distance and cell size (specifically, $2(A/\pi)^{1/2}$ where A is the area of the cell's image in pixels. This quantity is the diameter if the image is a circle). In separate experiments, the relationship obtained can be used to control the final fluorescence following electroporation by adjusting the tip-to-cell distance based on cell size. The relationship was applied successfully to A549 as well as DU 145 and PC-3 cells. Finally, *F*-tests show that the variability in the final fluorescence (following electroporation) is decreased when the tip-to-cell distance is controlled according to the derived relationship in comparison to experiments in which the tip–cell distance is a constant irrespective of cell size.

Electroporation[1–9] is a technique that uses electric fields to create nanopores (~1–10 nm)[10] in a cell's membrane, dramatically increasing its permeability. With dependence upon the conditions used for electroporation, the pores can either be transient or short-lived in reversible electroporation or long-lived in irreversible electroporation. Cell viability is maintained in reversible electroporation as the pores reseal in this case, whereas cell death occurs in irreversible electroporation as the pores do not reseal. This technique has been studied and applied for almost 3 decades. Over that time, it has been used to transport molecules, chiefly DNA, across cell membranes for a wide range of applications such as gene therapy,[11,12] molecular biology,[4,13] and clinical chemotherapy.[14]

[*]Corresponding author. Phone: +1(412)624-8520. Fax: +1(412)624-1668. sweber@pitt.edu..
[†]University of Pittsburgh.
[‡]Chalmers University of Technology.

SUPPORTING INFORMATION AVAILABLE Additional information as noted in text. This material is available free of charge via the Internet at http://pubs.acs.org.

There are two types of electroporation, namely, bulk electroporation and single-cell electroporation. In bulk electroporation, a batch of cells in suspension is exposed to a macroscopically uniform electric field of a few kilovolts per centimeter resulting in the permeabilization of many cells at the same time.[7,8,15–17] Neumann et al. in the early 1980s demonstrated gene transfection by bulk electroporation of mammalian cells.[4] Ever since, bulk electroporation has become a standard method for introduction of DNA into cells. However, bulk electroporation results in a distribution of outcomes among the cells in the suspension. It would be preferable, especially to study the membrane biophysics of cell permeabilization, to electroporate at the single-cell level.

Single-cell electroporation has shown promise, especially for application to natural, adherent cells, but is not as well studied as bulk electroporation. Single-cell electroporation should not be confused with bulk electroporation in which numerous cells are permeabilized but only individual cells are studied.[18–21] In single-cell electroporation, a localized field is applied to a single adherent cell or a cell in suspension flowing through a microfabricated device, while the neighboring cells are exposed to very low or no field.[22–28] Lundqvist et al. first demonstrated single-cell electroporation using carbon-fiber microelectrodes in 1998.[29] Since then, numerous other single-cell electroporation techniques using electrolyte-filled capillaries,[25,30] micropipets,[31] microfabricated chips,[32–34] and multiwalled carbon nanotubes[35] have been developed.

In bulk electroporation experiments, several workers have determined how to increase transport of DNA, dyes, and drugs across the cell membrane.[36–38] Normally, optimizing conditions for gene transfection in bulk electroporation has been the focus of studies.[4,39–41] Although transfection is of practical importance, it does not give a direct measure of transport across the membrane because transcription and translation involve many steps in addition to the transport of DNA such as DNA/membrane interaction, the translocation and migration of the plasmid into the cytoplasm, its passage into the nucleus, and the activation of expression. Other bulk electroporation studies have measured dye uptake to determine the effect of conditions on the success of electroporation.[37] A few bulk electroporation studies have quantified uptake of small fluorescent molecules using flow cytometry following bulk electroporation.[9,36] Small molecule uptake in bulk electroporation depends on electroporation parameters such as field strength, pulse length, number of pulses,[42–44] cell size, and shape[19] and other experimental conditions such as temperature, buffer,[45] etc. However, significant variability both in the observed result and in viability under constant conditions is generally observed in bulk electroporation.[44,46] Prausnitz and Canatella[47] used a statistical approach to predict the uptake of calcein and cell viability following bulk electroporation. Their prediction is based on a nonlinear regression approach to an empirical equation. On the basis of data for a single cell type, the experimental parameters important to permeabilization and viability were field strength, pulse length, and number of pulses. The empirical expression was useful for 60 different cell types. This rather impressive result solidifies the idea that it is the lipid bilayer's response to an electric field that controls bulk electroporation. We note that the model predicts the average behavior of a large population of cells. It is a telling measure of the inherent variability in the experiment that predictions within a factor of 2 of the observed result were considered satisfactory. To summarize, there are abundant quantitative studies of the electrical response of a cell in a homogeneous electric field and of the mass transport of molecules into an electroporated cell in bulk electroporation.

We are unaware of experimental reports that quantify mass transport out of cells following single-cell electroporation. An advantage of single-cell electroporation is the ability to relate a result to properties of the cell, not only to experimenter-controlled parameters. However, this dependence is hard to predict because single-cell electroporation lacks the symmetry of bulk electroporation in which suspended, nominally spherical cells are exposed to a nominally

homogeneous electric field. In the present work, we investigate mass transport from single cells following electroporation quantitatively The experimental method is based on first labeling thiols inside the cell with a maleimide-based fluorogenic reagent, Thioglo-1. As the most abundant thiol in the cell is reduced glutathione, GSH, we can say that the decrease in fluorescence intensity inside the cell following application of the pulse is predominantly due to the efflux of labeled glutathione from the cell. As the GSH–ThioGlo-1 conjugate has a formula weight of 684.7 Da, we view it as an indicator of the flux of freely diffusing molecules. Loss of fluorescence from diffusion of Thioglo-1 conjugates out of the cell was measured as a function of time. In a first set of experiments, which we will call set 1, the final fluorescence following electroporation and pore closing was correlated with experimental variables and parameters of the cell. In a second set of experiments, which we will call set 2, information from the first set was used to control the final fluorescence, which corresponds to a particular material loss from the cell, following electroporation. We show that a simple model developed for bulk electroporation describing the uptake of small molecules by cells in suspension[46] applies, following suitable modification, to the release of molecules from single, adherent cells on a nonconductive surface. We show that for constant experimental conditions (set 1), there is considerable variability in the extent of freely diffusing molecule release in single-cell electroporation. Finally, we show that, with statistical significance, we can control the magnitude of molecular flux from single cells and decrease the variability of the outcome if the size of the individual, adherent cell is taken into account in establishing the electroporation conditions (set 2).

EXPERIMENTAL SECTION

Materials

The chemicals used for buffer preparation were all analytical grade and were purchased from Sigma (St. Louis, MO). Thioglo-1 was purchased from Covalent Associates (Woburn, MA). Propidium iodide and calcein AM were purchased from Invitrogen/Molecular Probes (Eugene, OR). The cell lines A549, DU 145, and PC-3 were obtained from ATCC (Manassas, VA). Basal medium Eagle (BME), RPMI-1640, trypsin-EDTA, fetal bovine serum, L-glutamine, penicillin, and streptomycin were all obtained from Gibco-BRL (Carlsbad, CA). Milli-Q (Millipore Synthesis A 10, Billerica, MA) water was used. Extracellular buffer consisted of (mM) NaCl, 140.0; KCl, 5.0; $MgCl_2$, 2.0; $CaCl_2$, 2.0; D-glucose, 10; HEPES, 10.0; pH adjusted to 7.40.

Cell Culture and Staining

Human lung cancer A549 cells were cultured in BME supplemented with 10% fetal bovine serum, 100 U/mL penicillin, and 100 μg/mL streptomycin. DU 145 and PC-3 cells were grown in RPMI-1640 medium with 0.3 g/L L-glutamine, 10% fetal bovine serum, 100 U/mL penicillin, and 100 μg/mL streptomycin. Cells were grown as a monolayer in 75 mL cell culture flasks at 37 °C and 95% air/5% CO_2 (HERA cell incubator, Newtown, CT). Before the experiments, cells were plated on 35 mm, glass-bottom cell culture dishes (MatTek Corp., Ashland, MA) and were grown for up to 3 days. Experiments were performed on the second and third days following the cell plating. Before the experiments, the cells were stained with cell-permeable dye Thioglo-1 (2 μM in extracellular buffer) for 30 s at room temperature, then washed with extracellular buffer twice. Thioglo-1 is a maleimide-based reagent that gives a highly fluorescent product upon its reaction with active SH groups.[48,49] Cell dishes were mounted on the cell chamber (DH 35i culture dish incubator, Warner Instruments, Holliston, MA) and transferred to the stage of the microscope.

Probe Preparation

Fused-silica capillaries from Polymicro Technology (Phoenix, AZ) were used as a probe to perform electroporation experiments. Capillaries were pulled with a CO_2 laser puller (Sutter Instruments Co. P-2000, Novato, CA) to create reproducible capillaries with a short pulled tip having an inner diameter of ~5 μm. The final length of the capillaries was 15 cm.

Electroporation Setup

To electroporate a cell (Figure 1), the pulled tip of the capillary was submerged in the cell dish containing extracellular buffer. The other end of the capillary was placed in a vial filled with extracellular buffer. A platinum electrode placed in this vial was connected to the electroporator (ECM 830, BTX Instruments, San Diego, CA), and the electrical circuit was completed with a grounded platinum counter electrode placed in the cell dish. The counter electrode is a Pt wire situated at the periphery of the 35 mm diameter cell dish, typically about 15 mm from any electroporated cell. The capillary resistance was measured immediately prior to electroporation. The resistance determining circuit consisted of a synthesized function generator (SRS model DS 340, Stanford Research Systems, Inc., Sunnyvale, CA) and a lock-in amplifier (SRS model SR 830 DSP) which has an internal current-to-voltage converter. The function generator applied a continuous 2 V sine wave ac signal at 100 Hz across the aforementioned Pt electrodes with the electrolyte-filled capillary in place. The current resulting from the 2 V across the resistance of the capillary was measured by the lock-in amplifier. The resistance informed us about the status of the tip. Tips with an opening of 5 μm that are not clogged have a resistance of about 1.4×10^7 Ω. The test circuit is switched off during electroporation.

Fluorescence Imaging

Cells were observed through a 40× 1.3 NA oil immersion objective using an inverted microscope (Olympus, IX 71, Melville, NY) equipped with an HBO 100 W mercury lamp as the excitation source. For Thioglo-1, an Omega fluorescence cube (specially built, Omega, Brattleboro, VT) was used with filters for excitation at 378 nm and emission at 480 nm. For live/dead imaging, a triple band “Pinkel” filter set from Semrock (Rochester, NY) was used (exciter 1 387 nm, exciter 2 494 nm; exciter 3 575 nm; dichroic mirror, 394–414, 484–504, 566–586 nm; emitter, 457, 530, 628 nm). A CCD camera (Hamamatsu, ORCA-285, Bridgewater, NJ) imaged cells. The image collection frequency was 1 frame/s. Image processing was performed by the image acquisition software Simple PCI (Compix, Inc., Sewickley, PA).

Electroporation

There were two sets of experiments. In “set 1”, A549 cells were exposed to single pulses of duration 300–500 ms and magnitude 500 V. This will be referred as “pulsing” of the cells. The tip–cell distance, d_m (see Figure 1) was set at 2.0, 3.5, or 5.0 μm. At a time of 25 s from the initiation of the acquisition of images, the pulse was applied. Diffusive loss of fluorescent thiol (chiefly reduced glutathione) adducts from the cell was determined quantitatively with Simple PCI software. Further details of single-cell electroporation can be found elsewhere.[30,50]

In the second set (“set 2”), A549, PC-3, and DU 145 cells were used. Information from set 1 experiments was used to determine what value of d_m to use for a given cell, based on its size (the average diameters of the cells were A549, 25 μm; DU 145, 23.5 μm; and PC-3, 23 μm), to achieve a particular final fluorescence.

Cell Parameters

Cell parameters representing size, shape, and intensity were obtained by Simple PCI software. The size factors used were area, diameter, perimeter, and breadth. The area, *A*, is the total number of pixels in the image of a cell, the diameter is computed as $2(A/\pi)^{1/2}$, the perimeter is the distance traveled around the boundary of the cell, and the breadth is the average width of the cell's image. The shape factor is the aspect ratio (maximum length/maximum breadth). Intensity is the average gray level of the pixels in the object.

Measurement of Tip–Cell Distance

A 15 cm-long pulled capillary with a tip of ~5 μm in diameter was positioned near a cell using an MP-285 motorized micromanipulator from Sutter (Novato, CA). The capillary was first positioned at about a 45° angle with respect to the cell dish normal 5 μm above the surface (Figure 1). The distance between the capillary tip and the cell (d_m) was taken to be from the closest approach of the cell and the projection of the capillary image in the horizontal imaging plane.

Statistical Analysis

Fluorescence vs time data from 130 cells comprise the set 1 data. Stepwise forward and backward linear regression analyses were performed using the program STATA (Intercooled 9.0). The dependent variable was *K*, the ratio of mass transport rate constant to pore resealing rate constant (see below, eq 2). *K* is also related to the long-time (final or limiting) fluorescence intensity as shown in eq 1.

$$K=\ln\frac{F^0}{F_f} \tag{1}$$

where F^0 is the fluorescence intensity at the time of the application of the pulse before any decrease caused by mass transport out of the cell and F_f is the final fluorescence at long times. The independent variables used in the regression were the cell parameters area, diameter, perimeter, breadth, aspect ratio, and intensity and the experimental conditions, d_m and pulse duration. The cell parameters were transformed to get a normal distribution. The transformations are shown in Table 1. Regression analysis was based on the transformed variables.

Predictive Electroporation Experiments

In order to validate the regression results, set 2 electroporation experiments were performed again on the A549 cell line. Further, to validate our results for different cell lines, experiments were performed on two more cell lines: prostate adenocarcinoma cell line PC-3 and prostate cancer cell line DU 145. For this set of experiments we fixed the percent fluorescence intensity loss $100(1 - F_f/F^0)$, which we will call $\Delta F\%$. For example, in the case of the PC-3 cell line, cells were pulsed to achieve a 50% loss. In order to do so, the diameter of the cell to be pulsed was first measured using the Simple PCI software, then according to eq 4 the d_m at which the cell should be pulsed was determined. Similarly, experiments were performed on A549 cells to obtain $\Delta F\%$ equal to 20%, and 40%, and on cell line DU 145 to obtain $\Delta F\%$ equal to 40%.

Cell Viability Assay

Following electroporation experiments, live/dead analysis was performed on the cells. The buffer in the cell dish was replaced by 2 mL of fresh growth medium. The cells were allowed 5–6 h of recovery in the 37 °C incubator with 95% air/5% CO_2, followed by a 30 min staining with 2 μM (each) calcein AM and propidium iodide. Cell survival percentage was calculated

for each experimental condition based on this live/dead assay. It is important to note that a measurement of cell viability was made on each cell that was electroporated.

RESULTS AND DISCUSSION

Buffer Composition

In the present work, extracellular buffer (140 mM Na^+, 5 mM K^+) was used to perform the experiments as opposed to intracellular buffer (140 mM K^+, 5 mM Na^+) used in our previous work.[30,50] The range of pulse durations used in the previous experiments[30,50] performed with intracellular buffer was 50–300 ms at 500 V. The range of pulse durations used in the current work with extracellular buffer was 300–500 ms at 500 V. When extracellular buffer at pulse durations below 300 ms was used, the electroporation success for A549 cells was very low (<20%). Moreover, we found that the survival rate was higher with extracellular buffer as compared to intracellular buffer under the same set of experimental conditions. For example, at pulsing conditions of 300 ms and d_m of 2 μm, the survival rate with intracellular buffer was only ~0–5%, whereas in the case of extracellular buffer, the survival rate was ~65%. At longer distance, e.g., at pulse duration of 300 ms and d_m of 5 μm, the survival rate with intracellular buffer was 60%, whereas in the case of extracellular buffer, it was 95%. Thus, we have used only extracellular buffer in this work.

Fluorescence Intensity vs Time

In both set 1 and set 2 experiments, the function given in eq 2 was fitted to fluorescence intensity vs time curves.

$$F = F^0 e^{(-kt)} e^{[K(e^{-\alpha t}-1)]} \quad (2)$$

Here F is the fluorescence intensity at time t, F^0 is the fluorescence intensity at time zero when the pulse is applied, k is the photobleaching rate constant, $K = M/\alpha$ where M is the first order rate constant for transport of Thioglo-1 labeled molecules out of the cell, and α is the first order pore resealing rate constant. This equation results from incorporating a photobleaching term into the equation from Puc et al.[46]

Equation 2 incorporates the assumption that concentration polarization within the cell is minimal. We think that this is justified. The time scale over which the fluorescence intensity changes, and thus over which the intracellular concentration of thiol adducts changes, is on the order of 10 s. The relaxation time for a concentration perturbation in a sphere is approximately $a^2/15D$ (a is the sphere radius and D is the solute diffusion coefficient).[51] We estimate the diffusion coefficient of the Thioglo adduct of GSH in water to be 3×10^{-10} m^2 s^{-1}. Diffusion coefficients in the cytoplasm for noninteracting species (dextrans, ficolls) of a similar molecular size as the Thioglo adduct of GSH are about ¼ of the magnitude of the diffusion coefficients in free solution.[52,53] We thus estimate the relaxtion time in the cell to be on the order of 10^{-1} s, which is significantly smaller than the time over which concentrations change due to electroporation-induced flux. Thus, concentration polarization within the cell is not likely to influence the mass transport of low-molecular weight solutes out of the cell.

A program written in Mathcad (Mathsoft, Cambridge, MA) was used to fit decay curves, to estimate the parameters k, K, and α, and provide a goodness of fit R^2. Figure 2 gives an example of eq 2 fitted to a set of data. Here, the circles represent the data from a cell that was pulsed for 300 ms with a cell-to-capillary tip distance of 3.5 μm. The solid line is the best fit that was obtained using the Mathcad program. Table 2 gives a list of parameter definitions.

In initial explorations of the curve-fitting procedure, we used eq 3.

$$F = F^0 e^{(-kt)} e\left[\frac{M}{\alpha}\left(e^{-\alpha t} - 1\right)\right] \quad (3)$$

which, except for the photobleaching term, directly reflects the derivation of Puc et al.[46] It was found that M and α were somewhat correlated (the correlation coefficient between M and α arising from the nonlinear fitting, $\rho_{M\alpha}$, is 0.48). We repeated the nonlinear curve fitting with the ratio M/α replaced by the new parameter K. We then found no correlation between the fit parameters K and α ($\rho_{K\alpha} = -0.06$). By minimization of the correlation between these two fit parameters, the error in the result is also minimized. We should mention that K and α are not "adjusted" to compensate for photobleaching. Rather, the photobleaching rate constant is one of the parameters determined along with K and α. It turns out that the parameter K is useful in its own right. It is related to the fraction of the cell's final fluorescent contents, as shown above in eq 1. The value of K is important because it is a time-independent result of electroporation, the variability of which we seek to control. Our goal is to explain the variability (set 1 experiments) and then use that understanding to predict the result (set 2 experiments).

Set 1 Experiments

Recall that set 1 experiments represent a survey of $\Delta F\%$ for a set of cells of various sizes and shapes and of various tip–cell distances and pulse times, where $\Delta F\%$isthe percent fluorescence intensity loss 100 $(1 - F_f/F^0)$. In this set of experiments, the tip–cell distance was set arbitrarily for any given cell. A histogram of $\Delta F\%$ for all the cells pulsed at 2 μm d_m is shown in Figure 3. The average $\Delta F\%$ for these cells was 53%, with a standard deviation of percent loss in intensity ($\Delta F\%$) of 24%. The wide distribution of $\Delta F\%$ shows that there is a large variability in the outcome even when the tip–cell distance is constant.

In order to understand what variables affect K, we did multiple linear regression of K on the transformed independent variables pulse duration, tip–cell distance d_m, and the cell parameters in Table 1. The "size" (parameters area, diameter, perimeter, and breadth) are all highly correlated, but we do not know which is a better predictor (if any) of K. Thus, we used stepwise regression. The results from stepwise forward and backward linear regression of K on the transformed variables (Table 1) are shown in Table 3 and eq 4. There is significant relationship ($R^2 = 0.30$, $p < 0.001$ for the coefficients of d_m and d_c^{-1}, = p 0.694 for the constant) between dependent variable K and independent variables d_m and cell diameter d_c (μm). The fact that cell-size parameters other than diameter do not appear in the regression should not be taken to mean that they are not important.

$$K = -0.175 d_m + \frac{27.8}{d_c} + 0.122 \quad (4)$$

Numerical simulations[50] show that the transmembrane potential induced in an electroporation experiment depends on the tip–cell distance, the polar angle from the long axis of the capillary, and the cell size. The cell-size dependence of the fraction of the cell's surface area that is electroporated is smaller in single-cell electroporation ($\propto d_c^{0.33}$) than in the bulk experiment ($\propto d_c^{1.0}$).[50] In the single-cell experiment, the most critical variable is d_m, as it governs the electric field at the cell for a given applied voltage and capillary length. Thus, it is gratifying to find that both d_c and d_m are significant predictors.

The regression results were used to make a contour plot of $\Delta F\%$ as a function of d_m and d_c (Figure 4). The contour plot shows that at a given d_m, a smaller cell has a larger $\Delta F\%$ than a larger cell. It is instructive to consider the likely spread of values of $\Delta F\%$ for a fixed d_m given

the cell size distribution shown in the Box plot in Figure 4. The Box plot in Figure 4 represents the distribution of cell sizes in percentiles: 5th, 25th, 50th, 75th, and 95th (12, 19, 22, 27, and 36 μm, respectively). It is apparent that the median cell is predicted to lose 50% of its fluorescence at a d_m of about 3.9 μm. The spread of expected values (5th to 95th percentile) of fluorescence loss is fairly high at any value of d_m. It is clear that fixing the capillary tip–cell distance, d_m, is not sufficient to tightly control the field strength at the cell and thus the outcome of electroporation.

Set 2 Experiments

In these experiments, we sought to predict Δ*F*%. Equation 4 can be used to estimate the right tip-to-cell distance for a desired concentration decrease (or increase if diffusive flux is inward rather than outward). If, for example, a fluorescence decrease of 50% is desired and the cell diameter is 22 μm, then the equation directs us to use a d_m of 3.9 μm. In Set 2, the tip–cell distance was adjusted for each cell to achieve a particular Δ*F*%. We performed additional electroporation experiments on A549 cells and also on PC-3 and DU 145 cells. Results are shown in Table 4 for three cell types and for several predicted values of Δ*F*%. For example, the top row shows results from our attempt to obtain a Δ*F*% of 20% from A549 cells. The 95% confidence interval for Δ*F*% for these cells was [15, 22]. In fact, for all cell lines (A549, DU 145, and PC-3), the predicted Δ*F*% lies within the 95% confidence interval of the observed Δ*F*%.

Figure 5 is a histogram of Δ*F*% for A549 cells electroporated in set 1 (d_m = 2 μm) and set 2 experiments. The large spread in set 1 experiments shows that there is a large variance in the results (histogram A). Histograms B and C in Figure 5 show that we were able to reduce this variance by taking d_c into account (eq 4) when setting d_m. To further verify this reduction in the variance between set 1 and set 2 experiments, an *F*-test was performed between set 1 and each of the set 2 intensity loss observations. The results are shown in Table 5. The *F*-test results show that the variances in set 2 experiments were reduced significantly ($p < 0.05$) for all cell types. This is strong evidence that we can predict Δ*F*% by controlling d_m in accordance with eq 4.

In our previous research (using high K^+ buffer), we investigated conditions leading to successful electroporation and cell viability. The observations were binary in nature, i.e., either a cell was electroporated or it was not. In those experiments, we observed a large variability (e.g., the average Δ*F*% for all cells electroporated at 2 μm d_m was 55% with a standard deviation of 30%) in success and survivability at a given set of conditions.[30,50] We found that cell size and shape were significant factors in controlling success and survivability. Thus, at constant experimental conditions, the natural variability of the cells led to variability in the outcome. Nonetheless, we found conditions (experimental and cell parameters) at which we could maximize cell permeabilization and survivability. The present work goes one step beyond that. We have quantified the degree of electroporation. Also, we have not only found one of the factors that induces variability in the experiments but have also been able to reduce this variability by controlling the d_m according to eq 4. We note also, see Table 4, that the survival rate for the set 2 experiments is quite acceptable.

The statistical results in Tables 4 and 5 show two things. Table 4 demonstrates that taking into account the cell size in setting the tip–cell distance is critical to achieving a particular Δ*F*% on average. Table 5 demonstrates that taking into account the cell size in setting the tip–cell distance significantly reduces the variability of the outcome of electroporation (in terms of Δ*F* %). The experimental significance of the reduction in variance is a decrease in the number of experiments required to achieve a particular standard error of the mean given a particular experimental variability. Thus, with statistical rigor, we have demonstrated the advantage of distance control based on cell size in single-cell electroporation. However, it is also true that

the variability is still rather large. At this point, we do not know the cause of the variability, although it is by now well-known that cell-to-cell variability is to be expected in single-cell experiments of any sort. It is very likely that the parameter *K* depends on aspects of cell physiology that we do not now control. For example, we do not control for the number of passages of the cells or where the cells are in the cell cycle.

Origin of the Dependences Observed

It is interesting to pursue the origin of eq 4 from a causal rather than an observational (regression) perspective. Transient permeabilization in an electric field results when the transmembrane potential exceeds a critical value. Estimates of the critical value vary, but we have found that the value established by Teissie and Rols[54] of 250 mV is consistent with our observations.55 We have also previously determined the fraction of a hemispherical cell's exposed area ($\pi d_c^2/2$) that has a transmembrane potential greater than the critical value in single-cell electroporation with an electrolyte-filled capillary.[30] We define f_p as the fraction of the cell's surface area that has a transmembrane potential greater than or equal to the critical value at $t = 0$ (i.e., before the electrical conductance of the membrane increases because of the increased porosity). This permeabilized fraction, f_p is a function of tip–cell distance and of cell diameter.[50] The area of a cell that is permeabilized contributes to the efflux of a chemical species through the membrane.[43] A simple first order rate constant for the loss of material from a cell can be given as

$$M = \frac{A}{V}P \tag{5}$$

where *A* is the permeabilized area of the cell, *V* is the cell's volume, and *P* is the permeability of the solute through the (porated) membrane. The permeabilized area, *A*, is equal to the product of the cell's surface area, $\pi d_c^2/2$, and the fraction of the area that is permeabilized. The permeabilized area is thus $\pi/2 f_p d_c^2$. The cell's volume is $\pi d_c^3/12$.

We can thus write

$$M = \frac{6 f_p P}{d_c} \tag{6}$$

This mass transport coefficient is the same as that in Puc et al. mentioned above. It is the mass transport coefficient in the presence of the field, assumed constant. Recall from eq 3 that the time dependent part of the dynamics (pore resealing) is embodied in the time variable, the parameters *M*, α, and *K* are time-independent. We also assume here that the mass transport occurs solely by diffusion (e.g., not by electrophoresis) because we do not see experimentally an instantaneous drop in fluorescence at the time the pulse is applied (called "*g*" in Puc et al.). The computed values of f_p (called FEA in Figure 6 of Agarwal50) fit well to second order polynomials in d_m (see Supporting Information, Table S1). Using these polynomials, we calculated values of the term $6f_p/d_c$. This term is well-described by eq 7 ($R^2 = 0.87$, *p* values for coefficients of d_m and d_c^{-1} are <0.0001, for the constant, $p = 0.24$, see Supporting Information, Table S2).

$$\frac{6 f_p}{d_c} = -2.16 \times 10^{-3} d_m + \frac{0.6228}{d_c} - 0.002\,62 \tag{7}$$

This dependence is remarkably similar to the dependence seen for K (eq 4 and Table 3). The magnitudes of the parameters cannot be compared directly for the two equations; however, the relative parameter values can be. We note that in both equations the coefficient of d_m is negative, the coefficient of d_c^{-1} is positive, and the constant term is statistically indistinguishable from zero (see Supporting Information, Table S2 for regression statistics for eq 7). Further, the ratios of the coefficients of d_c^{-1} to the coefficients of d_m are similar, on the order of 10^2.

It is possible to make an inference about the electroporation process from this similarity. The functional similarity of eqs 4 and 7 means that the ratio of the two equations is approximately constant (not dependent on the independent variables). Explicit computation of the ratio shows that the ratio is approximately constant except for large cells and long distances, cases in which there is little or no fluorescence loss. Algebraically, the ratio of the two quantities on the left-hand sides of eqs 4 and 7 is equal to P/α. We infer that this ratio is approximately constant.

Krassowska's group has developed a pore formation and closure model based on energies and measured or estimated parameters.[56] In this model, after the electric pulse is removed all pores rapidly shrink to same pore area, i.e., the minimum-energy radius, r_m. Hence, after removal of the electric field, cells reseal from the same minimum-energy radius r_m.[56,57] Thus, the pore resealing rate is considered to be a constant. Indeed, while our measured values vary over a range of values (~0.1–1 s^{-1}), values of α were not correlated with any experimental or cell parameter. If the pore resealing rate is approximately constant and the ratio P/α is approximately constant for all cells, then we can conclude that, under the conditions of our experiments, the permeability of the cell immediately after the potential is returned to zero (P) is approximately independent of electroporation and cell-based parameters. Further, as we know the ratio P/α, and α, we can estimate P. This is necessarily highly approximate, so only an order of magnitude estimate is justified. We define P as the ratio of diffusion coefficient to membrane thickness, D/l, multiplied by a porosity, ϕ. The porosity ϕ refers to the effective fraction of the electroporated area (itself a fraction of the cell's surface area) through which molecules pass. Using $D \sim 10^{-10}$ m^2 s^{-1}, $l \sim 4$ nm, $\alpha \sim 0.1$ s^{-1}, we obtain $\phi \sim 10^{-4}$, a reasonable value.[21,37]

One important application of our present work of controlled release of small molecules from single cells is in single-cell analysis. The analysis of cytoplasmic contents of single cells using microfluidics and separations has become an important research area.[58–63] This is because highly efficient and sensitive detection of the components in a single cell will explain important physiological processes and therefore improve our understanding of basic cellular processes. Generally, although not always,[64,65] in the process of single-cell analysis, the cell is destroyed. It would be helpful to be able to sample a cell's cytoplasm over time. Our present work is a major step in this direction as the ability to predict/control small molecular release will provide a better handle at reproducibility in single-cell small molecular release experiments.

Supplementary Material

Refer to Web version on PubMed Central for supplementary material.

Acknowledgments

This work was financially supported by the National Institutes of Health (Grant R01 GM066018), the Foundation for Strategic Research (SSF), Vetenskapsrådet (VR), and the Göran Gustafsson Foundation to whom we are grateful.

References

(1). Kinosita K Jr. Tsong TY. Biochim. Biophys. Acta 1977;471:227–242. [PubMed: 921980]

(2). Kinosita K Jr. Tsong TY. Proc. Natl. Acad. Sci. U.S.A 1977;74:1923–1927. [PubMed: 266714]
(3). Teissie J, Tsong TY. Biochemistry 1981;20:1548–1554. [PubMed: 6261800]
(4). Neumann E, Schaefer-Ridder M, Wang Y, Hofschneider PH. EMBO J 1982;1:841–845. [PubMed: 6329708]
(5). Sugar IP, Neumann E. Biophys. Chem 1984;19:211–225. [PubMed: 6722274]
(6). Bliss JG, Harrison GI, Mourant JR, Powell KT, Weaver JC. Bioelectrochem. Bioenerg 1988;20:57–71.
(7). Prausnitz MR, Bose VG, Langer R, Weaver JC. Proc. Natl. Acad. Sci. U.S.A 1993;90:10504–10508. [PubMed: 8248137]
(8). Pliquett U, Weaver JC. Bioelectrochem. Bioenerg 1996;39:1–12.
(9). Gift EA, Weaver JC. Cytometry 2000;39:243–249. [PubMed: 10738276]
(10). Weaver JC, Chizmadzhev YA. Bioelectrochem. Bioenerg 1996;41:135–160.
(11). Xie TD, Tsong TY. Biophys. J 1990;58:897–903. [PubMed: 2248994]
(12). Xie TD, Sun L, Tsong TY. Biophys. J 1990;58:13–19. [PubMed: 2200534]
(13). Zimmermann U, Riemann F, Pilwat G. Biochim. Biophys. Acta 1976;436:460–474. [PubMed: 1276224]
(14). Mir LM, Orlowski S, Belehradek J Jr. Paoletti C. Eur. J. Cancer 1991;27:68–72. [PubMed: 1707289]
(15). Teissie J, Eynard N, Vernhes MC, Benichou A, Ganeva V, Galutzov B, Cabanes PA. Bioelectrochemistry 2002;55:107–112. [PubMed: 11786352]
(16). Teissie J, Golzio M, Rols MP. Biochim. Biophys. Acta 2005;1724:270–280. [PubMed: 15951114]
(17). Gehl J. Acta Physiol. Scand 2003;177:437–447. [PubMed: 12648161]
(18). Sixou S, Teissie J. Bioelectrochem. Bioenerg 1993;31:237–257.
(19). Valic B, Golzio M, Pavlin M, Schatz A, Faurie C, Gabriel B, Teissie J, Rols M-P, Miklavcic D. Eur. Biophys. J 2003;32:519–528. [PubMed: 12712266]
(20). Gabriel B, Teissie J. Biophys. J 1999;76:2158–2165. [PubMed: 10096909]
(21). Pucihar G, Kotnik T, Miklavcic D, Teissie J. Biophys. J 2008;95:2837–2848. [PubMed: 18539632]
(22). Rae JL, Levis RA. Pfluegers Arch 2002;443:664–670. [PubMed: 11907835]
(23). Haas K, Sin W-C, Javaherian A, Li Z, Cline HT. Neuron 2001;29:583–591. [PubMed: 11301019]
(24). Olofsson J, Nolkrantz K, Ryttsen F, Lambie BA, Weber SG, Orwar O. Curr. Opin. Biotechnol 2003;14:29–34. [PubMed: 12565999]
(25). Nolkrantz K, Farre C, Brederlau A, Karlsson RID, Brennan C, Eriksson PS, Weber SG, Sandberg M, Orwar O. Anal. Chem 2001;73:4469–4477. [PubMed: 11575795]
(26). Sims CE, Meredith GD, Krasieva TB, Berns MW, Tromberg BJ, Allbritton NL. Anal. Chem 1998;70:4570–4577. [PubMed: 9823716]
(27). Huang Y, Sekhon NS, Borninski J, Chen N, Rubinsky B. Sens Actuators, A: Phys 2003;A105:31–39.
(28). Valero A, Post JN, van Nieuwkasteele JW, ter Braak PM, Kruijer W, van den Berg A. Lab Chip 2008;8:62–67. [PubMed: 18094762]
(29). Lundqvist JA, Sahlin F, Aberg MAI, Stromberg A, Eriksson PS, Orwar O. Proc. Natl. Acad. Sci. U.S.A 1998;95:10356–10360. [PubMed: 9724707]
(30). Agarwal A, Zudans I, Orwar O, Weber SG. Anal. Chem 2007;79:161–167. [PubMed: 17194134]
(31). Ryttsen F, Farre C, Brennan C, Weber SG, Nolkrantz K, Jardemark K, Chiu DT, Orwar O. Biophys. J 2000;79:1993–2001. [PubMed: 11023903]
(32). Huang Y, Rubinsky B. Sens. Actuators, A: Phys 2001;A89:242–249.
(33). Khine M, Lau A, Ionescu-Zanetti C, Seo J, Lee LP. Lab Chip 2005;5:38–43. [PubMed: 15616738]
(34). He H, Chang DC, Lee Y-K. Bioelectrochemistry 2006;68:89–97. [PubMed: 16039911]
(35). Rojas-Chapana J, Troszczynska J, Firkowska I, Morsczeck C, Giersig M. Lab Chip 2005;5:536–539. [PubMed: 15856091]
(36). Canatella PJ, Karr JF, Petros JA, Prausnitz MR. Biophys. J 2001;80:755–764. [PubMed: 11159443]
(37). Neumann E, Toensing K, Kakorin S, Budde P, Frey J. Biophys. J 1998;74:98–108. [PubMed: 9449314]

(38). Rols MP, Teissie J. Biophys. J 1990;58:1089–1098. [PubMed: 2291935]
(39). Faurie C, Golzio M, Phez E, Teissie J, Rols MP. Eng. Life Sci 2005;5:179–186.
(40). Maasho K, Marusina A, Reynolds NM, Coligan JE, Borrego F. J. Immunol. Methods 2004;284:133–140. [PubMed: 14736423]
(41). Tao W, Wilkinson J, Stanbridge EJ, Berns MW. Proc. Natl. Acad. Sci. U.S.A 1987;84:4180–4184. [PubMed: 3473500]
(42). Loste F, Eynard N, Teissie J. Bioelectrochem Bioenerg 1998;47:119–127.
(43). Rols M-P, Teissie J. Biophys. J 1998;75:1415–1423. [PubMed: 9726943]
(44). Gabriel B, Teissie J. Biochim. Biophys. Acta 1995;1266:171–178. [PubMed: 7742383]
(45). Djuzenova CS, Zimmermann U, Frank H, Sukhorukov VL, Richter E, Fuhr G. Biochim. Biophys. Acta 1996;1284:143–152. [PubMed: 8914578]
(46). Puc M, Kotnik T, Mir LM, Miklavcic D. Bioelectrochemistry 2003;60:1–10. [PubMed: 12893304]
(47). Canatella PJ, Prausnitz MR. Gene Ther 2001;8:1464–1469. [PubMed: 11593359]
(48). Fabisiak JP, Sedlov A, Kagan VE. Antiox. Redox Signal 2002;4:855–865.
(49). Kagan VE, Kuzmenko AI, Tyurina YY, Shvedova AA, Matsura T, Yalowich JC. Cancer Res 2001;61:7777–7784. [PubMed: 11691792]
(50). Agarwal A, Zudans I, Weber EA, Olofsson J, Orwar O, Weber SG. Anal. Chem 2007;79:3589–3596. [PubMed: 17444611]
(51). Glueckauf E. Trans. Faraday Soc 1955;51:1540–1551.
(52). Seksek O, Biwersi J, Verkman AS. J. Cell Biol 1997;138:131–142. [PubMed: 9214387]
(53). Luby-Phelps K, Castle PE, Taylor DL, Lanni F. Proc. Natl. Acad. Sci. U.S.A 1987;84:4910–4913. [PubMed: 3474634]
(54). Teissie J, Rols MP. Biophys. J 1993;65:409–413. [PubMed: 8369446]
(55). Zudans I, Agarwal A, Orwar O, Weber SG. Biophys. J 2007;92:3696–3705. [PubMed: 17351001]
(56). Smith KC, Neu JC, Krassowska W. Biophys. J 2004;86:2813–2826. [PubMed: 15111399]
(57). Saulis G. Biophys. J 1997;73:1299–1309. [PubMed: 9284298]
(58). Borland LM, Kottegoda S, Phillips KS, Allbritton NL. Ann. Rev. Anal. Chem 2008;1:191–227.
(59). Cannon DM Jr. Winograd N, Ewing AG. Annu. Rev. Biophys. Biomol. Struct 2000;29:239–263. [PubMed: 10940249]
(60). Bergquist J, Josefsson E, Tarkowski A, Ekman R, Ewing A. Electrophoresis 1997;18:1760–1766. [PubMed: 9372267]
(61). Han F, Wang Y, Sims CE, Bachman M, Chang R, Li GP, Allbritton NL. Anal. Chem 2003;75:3688–3696. [PubMed: 14572031]
(62). Meredith GD, Sims CE, Soughayer JS, Allbritton NL. Nat. Biotechnol 2000;18:309–312. [PubMed: 10700147]
(63). Stuart JN, Sweedler JV. Anal. Bioanal. Chem 2003;375:28–29. [PubMed: 12520431]
(64). Olefirowicz TM, Ewing AG. Anal. Chem 1990;62:1872–1876. [PubMed: 2240573]
(65). Woods LA, Gandhi PU, Ewing AG. Anal. Chem 2005;77:1819–1823. [PubMed: 15762591]

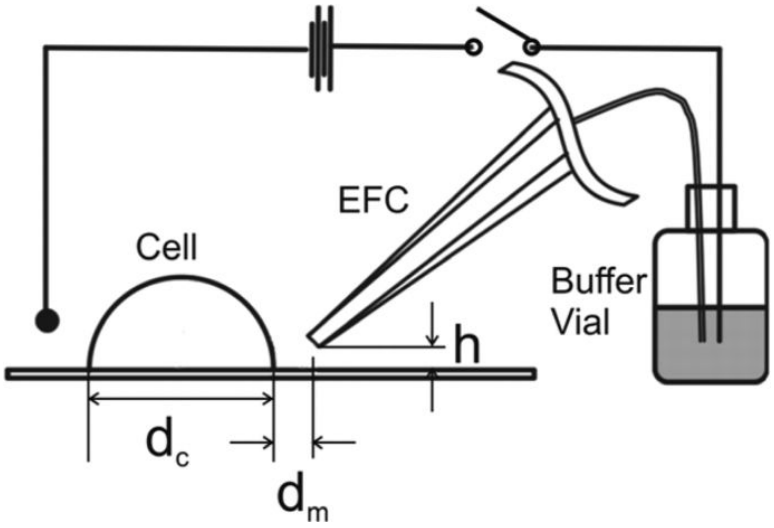

Figure 1.

Schematic diagram of the experimental setup. A culture dish containing adherent cells was mounted in a chamber on the microscope stage. A 15 cm long pulled capillary with a tip of ~5 μm in diameter was positioned near a fluorescent cell with the help of a micromanipulator. The capillary was first positioned at about a 45° angle with respect to the cell dish normal 5 μm (*h*) above the surface. The other end of the capillary was placed in a buffer-filled vial. The setup was connected to a high voltage power supply. Single fluorescent cells were exposed to single pulses of 500 V with pulse duration ranging from 300–500 ms. The tip–cell distance, d_m was set at 2.0, 3.5, or 5.0 μm. d_m was taken to be from the closest approach of the cell and the projection of the capillary image in the horizontal imaging plane. The counter electrode is a Pt wire situated at the periphery of the 35 mm diameter cell dish, typically about 15 mm from any electroporated cell.

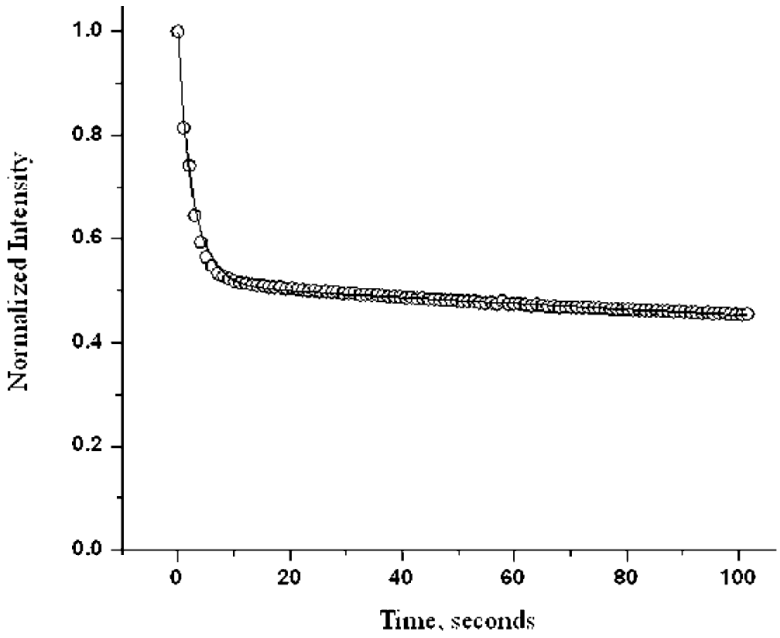

Figure 2.

A representative curve-fitting of the experimental data. The ◯ represent the experimental data (normalized fluorescence intensity). The experiment was performed on an A549 cell (set 1). The cell was pulsed for 300 ms with d_m=3.5 μm The pulse was applied at t = 0. The solid line is the best fit to the experimental data (R^2 = 0.99). The data was fitted to eq 1 using a program written in Mathcad.

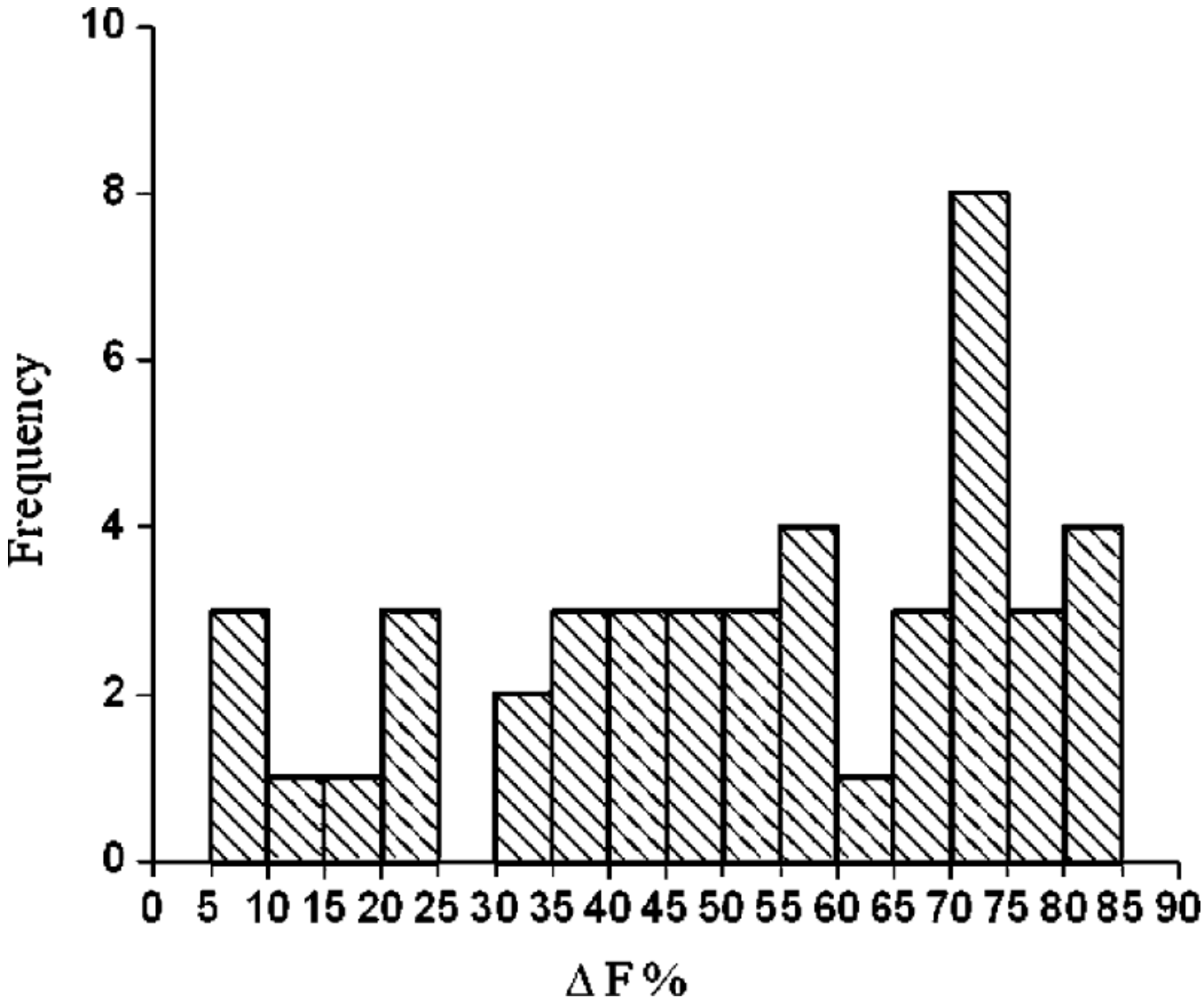

Figure 3.

Histogram of Δ*F*% for all the cells electroporated at 2 μm d_m in set 1 experiments. In set 1 experiments, A549 cells were exposed to single pulses of 500 V with pulse duration ranging from 300 to 500 ms. In this set of experiments, d_m was set arbitrarily for any given size or shape of the cell. The wide distribution in the Δ*F*% shows that there is a larger variability in the outcome. For the *x*-axis labeling, the second number which defines the interval is exclusive, whereas the first number is inclusive, e.g., for Δ*F* of 5–10%, the interval goes from 5.000 to 9.999.

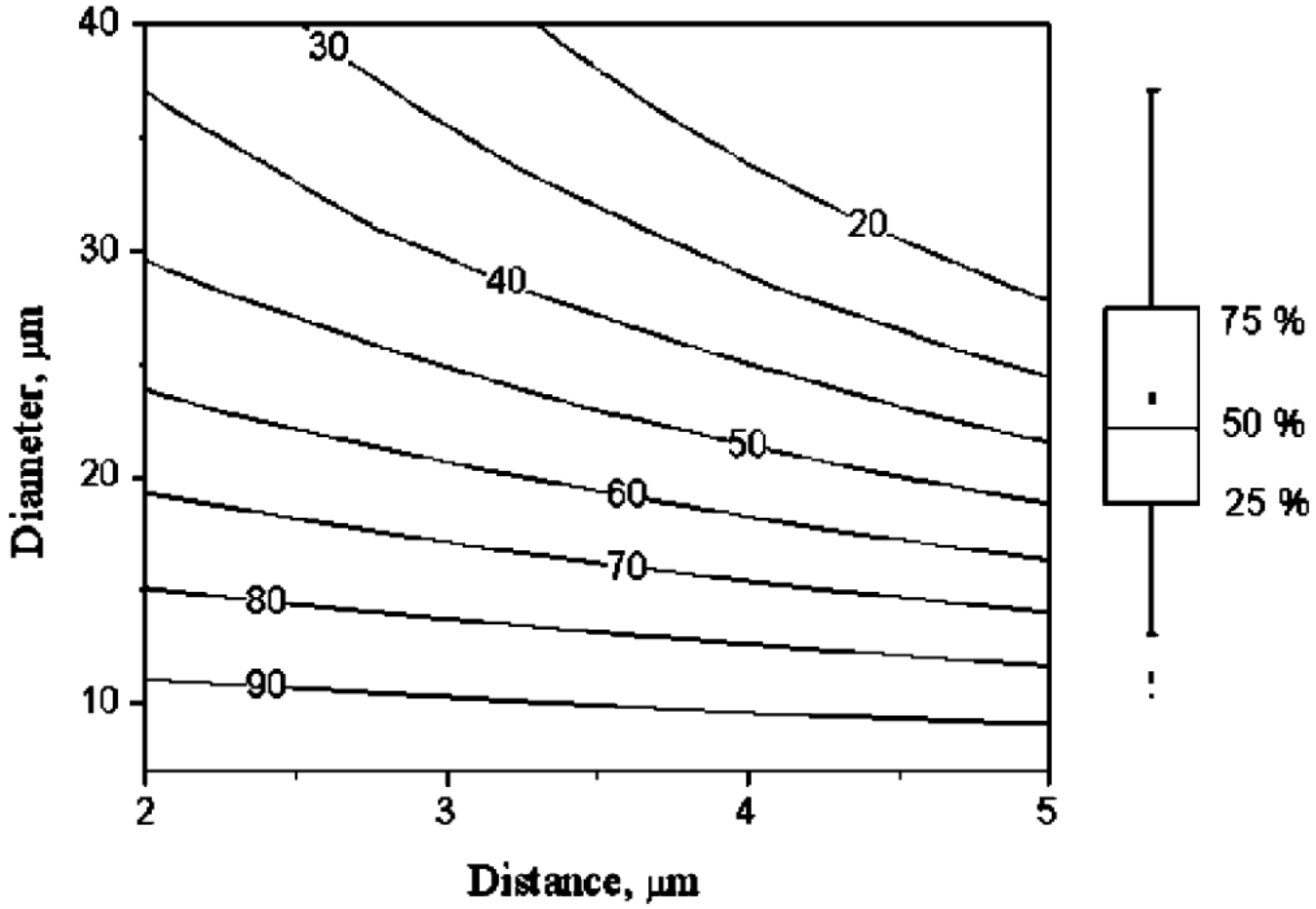

Figure 4.

Contour plot of Δ*F*% as a function of cell diameter (d_c) and cell–capillary tip distance (d_m). At a given d_m, a smaller cell has a larger Δ*F*% than a larger cell. As an example, a median cell is predicted to lose 50% of its fluorescence at a d_m of about 3.9 μm. The box plot gives the 5th, 25th, 50th, 75th, and 95th percentile of cell sizes corresponding to d_c 12, 19, 22, 27, and 36 μm.

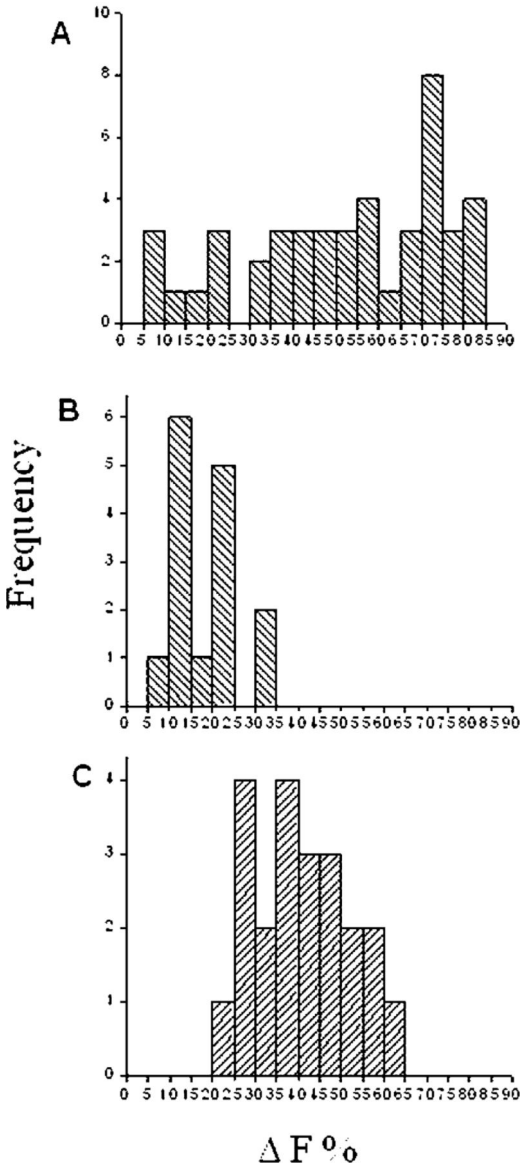

Figure 5.

Histograms of Δ*F*%. A549 cells electroporated in set 1 (d_m = 2 μm, pulse duration 300–500 ms) (A) and set 2 experiments (B, C). Histogram B represents cells electroporated to achieve Δ*F*% = 20%, and histogram C represents cells electroporated to achieve Δ*F*% = 40%. For the *x*-axis labeling, the second number which defines the interval is exclusive, whereas the first number is inclusive.

Table 1

Cell Variables and Their Transformations

variable (x)	transformation
area	$1/x$
diameter	$1/x$
perimeter	$1/\sqrt{x}$
breadth	$\sqrt{x}$
aspect ratio	$\sqrt{x}$
intensity	x^2

Table 2

List of Parameter Definitions

parameter	definition
k	photobleaching rate constant, s^{-1}
K	ratio of mass transport rate constant to pore resealing rate constant, unitless
α	pore resealing rate constant, s^{-1}
d_c	cell diameter, μm
d_m	distance between the capillary tip and the cell, taken from the closest approach of the cell and the projection of the capillary image in the horizontal imaging plane, μm (See Figure 1)

Table 3

Results of Linear Regression Analysis of K on Experimental Conditions and Cell Parameters[a]

	coefficient	standard error	*p* value
d_m	−0.175	0.036	<0.001
$1/d_c$	27.8	6.8	<0.001
constant	0.122	0.31	0.69

[a] Values of d_m and d_c are in micrometers.

Table 4

Expected ΔF%, Average ΔF% Observed, Standard Error of the Mean 95% Confidence Interval of the Mean, and Survival % for Cell Lines A549, PC-3, and DU 145

cell line (number of cells)	expected Δ*F*%	average Δ*F*% observed	standard error of the mean	95% confidence interval for the mean	survival %
A549 (15)	20	18	1.9	[15, 22]	100
A549 (21)	40	41	2.4	[36, 45]	95
DU 145 (15)	40	38	2.1	[34, 42]	100
PC-3 (15)	50	52	3.8	[44, 59]	86

Table 5

F-Test Results on Variance in Δ*F*% between Set 1 and Set 2 Experiments

cell line	expected Δ*F*%	df_1[a]	df_2[a]	F	*p* value (<)
A549	20	44	14	9.77	0.001
A549	40	44	20	4.22	0.001
DU 145	40	44	14	8.34	0.001
PC-3	50	44	14	2.43	0.05

[a] *df*, degrees of freedom.

Anal Chem. Author manuscript; available in PMC 2010 October 1.